Animal cells connected by nanotubes can be electrically coupled through interposed gap-junction channels

Xiang Wang, Margaret Lin Veruki, Nickolay V. Bukoreshtliev, Espen Hartveit, and Hans-Hermann Gerdes[1]

Department of Biomedicine, University of Bergen, 5009 Bergen, Norway

Tunneling nanotubes (TNTs) are recently discovered conduits for a previously unrecognized form of cell-to-cell communication. These nanoscale, F-actin–containing membrane tubes connect cells over long distances and facilitate the intercellular exchange of small molecules and organelles. Using optical membrane-potential measurements combined with mechanical stimulation and whole-cell patch-clamp recording, we demonstrate that TNTs mediate the bidirectional spread of electrical signals between TNT-connected normal rat kidney cells over distances of 10 to 70 μm. Similar results were obtained for other cell types, suggesting that electrical coupling via TNTs may be a widespread characteristic of animal cells. Strength of electrical coupling depended on the length and number of TNT connections. Several lines of evidence implicate a role for gap junctions in this long-distance electrical coupling: punctate connexin 43 immunoreactivity was frequently detected at one end of TNTs, and electrical coupling was voltage-sensitive and inhibited by meclofenamic acid, a gap-junction blocker. Cell types lacking gap junctions did not show TNT-dependent electrical coupling, which suggests that TNT-mediated electrical signals are transmitted through gap junctions at a membrane interface between the TNT and one cell of the connected pair. Measurements of the fluorescent calcium indicator X-rhod-1 revealed that TNT-mediated depolarization elicited threshold-dependent, transient calcium signals in HEK293 cells. These signals were inhibited by the voltage-gated Ca^{2+} channel blocker mibefradil, suggesting they were generated via influx of calcium through low voltage-gated Ca^{2+} channels. Taken together, our data suggest a unique role for TNTs, whereby electrical synchronization between distant cells leads to activation of downstream target signaling.

Cell-to-cell communication plays an important role in physiological processes of multicellular organisms. Diverse signaling pathways have been documented for the exchange of molecular information between cells. These include (*i*) the direct interaction of cell-surface molecules, (*ii*) the secretion of signaling molecules and their receptor-mediated uptake by target cells, and (*iii*) the direct transport of molecules through gap junctions. In addition to the exchange of signaling molecules, cells also communicate via electrical signals, where electrical coupling of cells via gap junctions is crucial for information processing and synchronization. Recent studies implicate electrical signaling in developmental processes, such as the establishment of left-right pattern in embryos (1), tail regeneration of *Xenopus* (2), and wound healing (2).

Some years ago, a new route of intercellular communication, based on the formation of tunneling nanotubes (TNTs) or similar structures that connect cells over long distances, was identified (3, 4). These membrane tubes, typically 50 to 200 nm in diameter with lengths up to several cell diameters, contain F-actin and, as a characteristic property, lack contact to the substratum (5). Subsequently, a growing number of cell types have been shown to form and use TNTs for the exchange of diverse cellular components, such as endocytic vesicles, mitochondria, plasma membrane proteins, and cytoplasmic molecules (6, 7). Pathogens, such as HIV (8, 9) and prions (10), have also been found to spread via TNT-like structures. The increasing number of functions attributed to TNTs (6, 7, 11), in conjunction with the recent finding that these struc-

tures exist in vivo (12), suggests important roles in intercellular communication of TNTs under physiological conditions.

The question arises as to whether, in addition to the exchange of molecules, TNTs also convey electrical signals between distant cells. The demonstration that artificial membrane nanotubes with a similar diameter as TNTs are efficient conductors of electrical currents (13) suggests that TNTs may also accomplish electrical cell-to-cell coupling. To investigate this theory, we combined optical membrane-potential measurements and electrophysiological methods to analyze electrical signals between TNT-connected cell pairs. Our results demonstrate that TNTs can mediate electrical coupling between distant cells and provide evidence that gap junctions participate in this long-distance coupling. Furthermore, we show that the electrical signals transferred from one cell to another are sufficient to induce a transient calcium elevation in the recipient cell by activating low voltage-gated Ca^{2+} channels.

Results

Mechanical Stimulation-Induced Depolarization Spreads Through TNT Connections Between Normal Rat Kidney Cells. To identify TNTs in normal rat kidney (NRK) cells, we used differential interference contrast (DIC) microscopy to avoid phototoxic damage to these fragile structures. Only straight intercellular connections (>10 μm in length) without contact to the substratum and lacking a midbody structure were considered. This process eliminated filopodia-based cell-to-cell contacts and dividing cells from our analysis. Time-lapse imaging demonstrated that all TNTs between NRK cells formed by cell dislodgement (Fig. S1) (*n* = 54 formation events). To exclude potentially complex circuits during our measurements, we selected only TNT-connected cell pairs devoid of contact to other cells (Fig. 1*A*, DIC images). Depolarization of single cells was induced by mechanical stimulation and measured as an increase in fluorescence of a preloaded membrane potential sensitive dye, bis-(1,3-dibutylbarbituric acid) trimethine oxonol [DiBAC₄(3)]. The fluorescence of both stimulated cells and TNT-connected cells increased after mechanical stimulation (Fig. 1*A*, pseudocolored intensity images). Cells lacking physical connections to the stimulated cell pair did not display an increase in fluorescence. This finding excluded the possibility that the depolarization spread by diffusion of molecular signals between cells. The amplitude of depolarization in the recipient cell was always lower than that of the stimulated cell (Fig. 1*B*), suggesting that the TNT-dependent depolarization signal moved passively from one cell to the other. As a control for our optical measurements, abutting NRK cells (that is, cells whose plasma membranes displayed a large area of contact) always showed strong electrical coupling in addition to the intercellular spread of Cascade Blue, a dye injected into the stimulated cell during mechanical stimulation
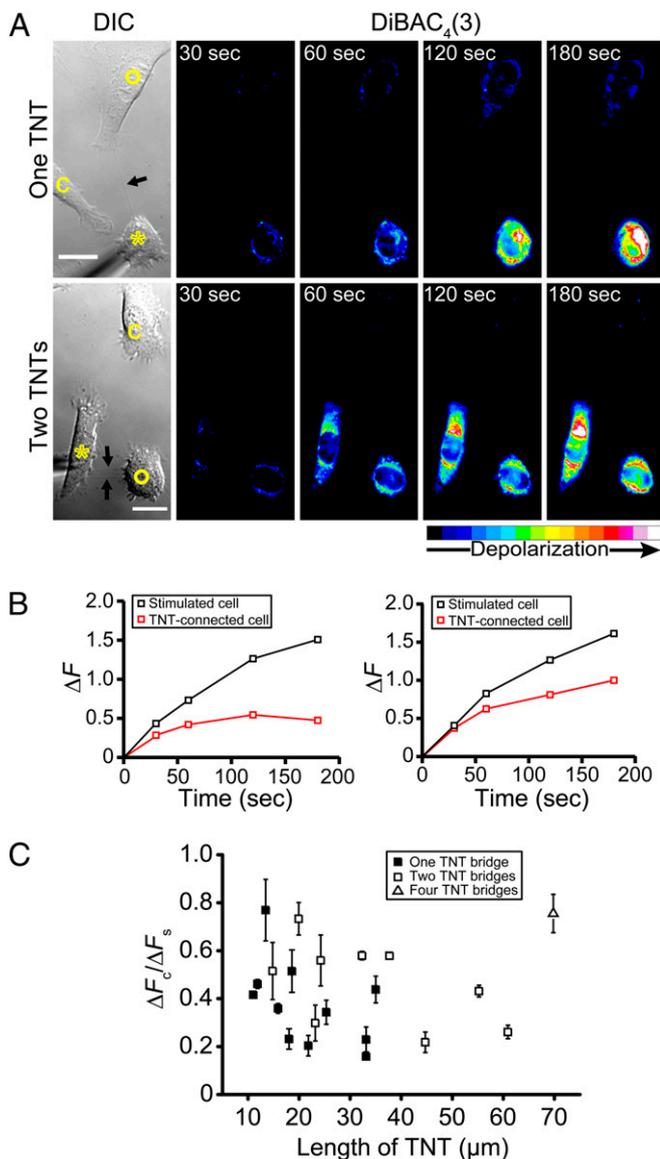
Fig. 1. Depolarization signals spread between TNT-connected NRK cells. (*A*) The DIC images show the mechanically stimulated NRK cells (asterisks), TNT-connected cells (open circles), TNTs (arrows), and control cells (c). The pseudocolored intensity images, generated by subtraction of the image before stimulation, show DiBAC$_4$(3) fluorescence increase at indicated times after mechanical stimulation for one (*Upper*) and two TNT-connections (*Lower*) per connected cell pair. The color bar indicates relative level of depolarization. (Scale bars, 20 μm.) (*B*) Quantification of the relative membrane potential changes of the stimulated cell (ΔF_s) and the TNT-connected cell (ΔF_c) for one (*Left*) or two TNT-connections (*Right*) as shown in A. (C) Correlation of the electrical coupling efficiency (ΔF_c/ΔF_s) and the TNT length. Each datapoint corresponds to the mean of the ΔF_c/ΔF_s values of TNT-coupled NRK cell pairs (n = 21) acquired at 30, 60, 120, and 180 s. Error bars are ± SEM.

(Fig. S2*A*). In addition, the presence of immunostaining against connexin 43 at the interface of these abutting cells suggested that NRK cells expressed functional gap junctions (Fig. S2*B*). We never detected the diffusion of Cascade Blue between TNT-connected cells, even after 20 min of dye injection (Fig. S2*C*), indicating that the passive diffusion of small molecules such as Cascade Blue through TNT structures is strongly reduced.

Interestingly, cells connected by one TNT to a stimulated cell showed weaker depolarization signals than cells connected by two shorter TNTs (Fig. 1*A* and red curves in Fig. 1*B*). To elucidate the relationship between the strength of electrical coupling and the

length of the TNT, we analyzed cell pairs connected with TNTs of varying length. Measurement of 31 TNT-connected NRK cell pairs revealed that 25 (~80%) were electrically coupled. The coupling efficiency, calculated as the ratio of depolarization between a single TNT-connected cell and the stimulated cell (ΔF_c/ΔF_s), decreased with increasing TNT length (Fig. 1*C*) (r_s = −0.60, P = 0.038, Spearman's correlation analysis). As noted above, cell pairs connected by more than one TNT displayed stronger electrical coupling compared with cell pairs connected by one TNT of similar length (Fig. 1*C*, open symbols). This finding implies that multiple TNT-connections between cells can operate as parallel conduits for the spread of electrical signals. Thus, the strength of electrical coupling between TNT-connected cells is determined by both the length and number of TNT-connections between them.

Whole-Cell Patch-Clamp Recording Reveals Bidirectional Electrical Coupling Between TNT-Connected NRK Cells. To further characterize TNT-dependent electrical coupling, we performed simultaneous, dual whole-cell voltage-clamp recordings from pairs of TNT-connected NRK cells. Electrical coupling was tested by applying voltage steps to one cell and recording current responses in both cells (Fig. 2*A*). A hyperpolarizing voltage applied to one cell resulted in an inward current in that cell and an outward current in the TNT-connected cell, whereas a depolarizing voltage applied to one cell resulted in an outward current in that cell and an inward current in the connected cell (Fig. 2 *B* and *C*, *Left* and *Center*). To estimate the junctional conductance (G_j), we applied a series of depolarizing and hyperpolarizing voltage pulses to the stimulated cell. By plotting junction current (I_j) versus junction voltage (V_j), we calculated G_j as the slope of a straight line fitted to the I_j–V_j relationship (Fig. 2 *B* and *C*, *Right*). Both directions of measurement showed very similar conductance (Fig. 2*D*), indicating nonrectifying, bidirectional electrical coupling. Thus, the conductance for a cell pair was calculated as the average of the conductance values measured in each direction (14). All TNT-connected cell pairs tested displayed fast electrical coupling with an average conductance of 566 ± 129 pS (range 55–1,341 pS, n = 12). The electrical coupling was abolished if the TNT broke during recording. As expected, given the presence of gap junctions in NRK cells, recording from pairs of cells in which the cell bodies or filopodia were in direct physical contact always resulted in strong electrical coupling, with higher conductances (8.9 ± 1.9 nS, range 1.8–25 nS, n = 12) compared with TNT-connected cell pairs. Cell pairs without physical contact never exhibited electrical coupling (n = 4). The conductance between single TNT-connected cell pairs decreased with increasing length of the TNTs (Fig. 2*E*) (r_s = −0.83, P = 0.0029, Spearman's correlation analysis). Additionally, two cell pairs that were connected with two TNTs each displayed higher conductance values compared with cell pairs connected by a single TNT-connection of similar length (Fig. 2*E*, open symbols). The results from these electrophysiological experiments are consistent with our optical membrane-potential measurements.
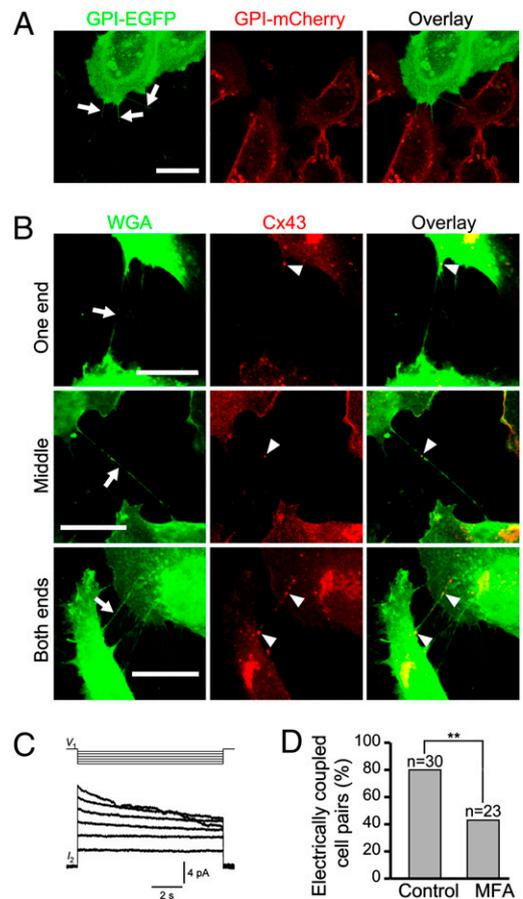
Cx43 Participates in the TNT-Dependent Electrical Coupling of NRK Cells. Our results raised the question of the structural basis for the observed TNT-dependent electrical coupling. Structural models have been proposed previously with the possibility that TNTs are continuous with the membranes of both cells of a pair or with only one of the cells (3, 8). To test for TNT-mediated membrane continuity, we analyzed mixed populations of NRK cells transfected with fluorescent plasma membrane markers. One population, expressing GPI-EGFP, was cocultured with a second population expressing GPI-mCherry. Confocal live-cell fluorescence microscopy revealed that all TNTs were labeled by a single marker (Fig. 3*A*) (n = 50). This finding indicated that GPI-anchored plasma membrane markers did not diffuse freely between TNT-connected NRK cells and suggested that the TNTs are continuous with only one of these cells. The likely existence of a plasma membrane at the other end of a TNT bridge suggests that a mechanism for the electrical coupling via a TNT could be the presence of gap junctions at points of contact between the cells. To test this theory, we immunolabeled TNT-connected NRK cell pairs with an antibody
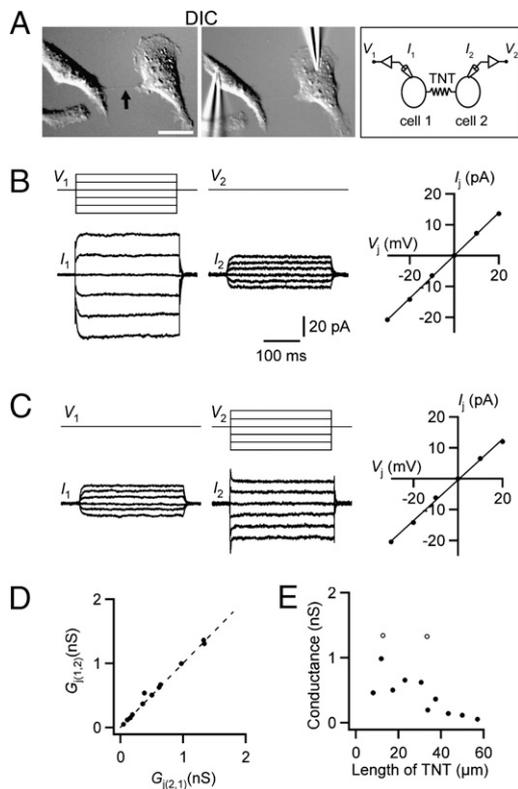
Fig. 2. Simultaneous voltage-clamp recordings from TNT-connected NRK cell pairs reveal bidirectional electrical coupling. (*A*) DIC image of TNT-connected NRK cell pair before (*Left*) and during (*Center*) electrophysiological recording; arrow indicates the TNT. Diagram (*Right*) illustrates recording configuration with V_1 and V_2 representing the voltage injected into cell 1 and cell 2, respectively, and I_1 and I_2 representing the currents measured in cell 1 and cell 2, respectively. (Scale bar, 20 μm.) (*B*) With the TNT-connected NRK cell pair in *A* in voltage-clamp (V_{hold} = 0 mV), a series of 300-ms voltage pulses (V_1) of −30 mV to +10 mV (in 10-mV increments; illustrated in upper left traces) were applied to cell 1 while current responses were recorded from both cells (I_1 and I_2; lower left traces). A hyperpolarizing (or depolarizing) voltage pulse applied to cell 1 results in an inward (or outward) current in cell 1 and an outward (or inward) current in cell 2. (*Right*) The current-voltage relationship for the junctional current (I_j) versus the junctional voltage (V_j) is shown. Datapoints have been fit with a straight line (slope = G_j). (*C*) Same as in *B*, but voltage steps are applied to cell 2. (*D*) Comparison of G_j in each direction indicates nonrectifying electrical coupling, ($G_{j(12)}$ for cell 1, $G_{j(21)}$ for cell 2). The dashed line has a slope of one. (*E*) Relation between conductance of TNT-coupled NRK cells (n = 12) and length of the TNT. Open dots represent cell pairs connected with two TNTs.

against Cx43. Punctate Cx43 signals were observed on 78% of all TNT structures (n = 54). The Cx43 immunolabeling was usually confined to one position of the TNT structure (Fig. 3*B*, *Top* and *Middle*) (n = 35), but was sometimes observed at both ends of the TNT (Fig. 3*B*, *Bottom*) (n = 7). This result was most likely because of the presence of two or more TNTs located very closely together. The absence of Cx43 labeling in 22% of the TNTs analyzed here is consistent with our finding that 20% of NRK cells were not electrically coupled. Furthermore, this finding indicates that TNTs in NRK cells form independently of gap junctions.

If Cx43 mediates the observed TNT-dependent electrical coupling, the conductance should display voltage-dependent sensitivity, as previously demonstrated for Cx43-containing gap junctions (15). We tested for voltage-sensitivity of the coupling with relaxation experiments by applying 10-s long hyperpolarizing voltage pulses (V_j = −20 to −120 mV, 20-mV steps) to one cell of a TNT-connected cell pair from a common holding potential of 0 mV. For transjunctional voltages higher than 60 mV, we observed a time-

Fig. 3. Gap junctions participate in TNT-dependent electrical coupling of NRK cells. (*A*) Membrane markers do not freely diffuse between TNT-connected NRK cells. Mixed populations of GPI-EGFP- and GPI-mCherry-labeled cells were imaged after 24 h of coculturing. Three TNTs (arrows) connecting GPI-EGFP (green)- and GPI-mCherry (red)-expressing cells, respectively, are labeled throughout their entire length with only GPI-EGFP. (*B*) Cx43 colocalizes with TNT structures of NRK cells. Cells were fluorescently labeled using wheat germ agglutinin (WGA) (green) and anti-Cx43 (red) as indicated. The confocal images show distinct signals of Cx43 immunolabeling (arrowheads) at one end (n = 24), in the middle (n = 11), or at both ends (n = 7) of a TNT (arrow). (*C*) Relaxation experiments determine steady-state voltage sensitivity of TNT-dependent electrical coupling of NRK cells. A series of 10-s hyperpolarizing voltage steps between −20 mV and −100 mV (in 20-mV increments) were applied to one cell (V_1, Upper). The resulting current responses in the nonstepped cell show relaxation when the voltage difference is > 60 mV (I_2, Lower). Note the relaxation of I_2 at voltage steps ≥ −60 mV. (*D*) TNT-dependent depolarization-coupling is inhibited by MFA. NRK cells were incubated with 25 μM MFA for 20 min. After one cell was mechanically stimulated, the DiBAC$_4$(3) fluorescence of TNT-connected cells was measured. The graph shows the percentage of coupled-cell pairs in the absence (control) and presence of MFA (P = 0.009, Fisher's Exact Test). The threshold applied to identify electrically coupled, TNT-connected cells is described in *Materials and Methods*. n, number of cell pairs analyzed. (Scale bars, 20 μm.)

dependent decrease of the junctional current in the recorded cell (Fig. 3*C*), indicating a corresponding time-dependent decrease of the conductance. Between subsequent voltage pulses, cells were returned to 0 mV for 30 s to allow for recovery from the voltage relaxation. All TNT-connected NRK cell pairs (n = 5) tested displayed some degree of voltage sensitivity, although complete datasets were difficult to obtain because of the fragility and short lifetime of TNTs (5) during these longer-lasting recordings. Furthermore, the percentage of TNT-dependent electrically coupled NRK cells, assessed by an increase in DiBAC$_4$(3) fluorescence following mechanical stimulation, decreased in the presence of 25 μM

Wang et al.

meclofenamic acid (MFA), a blocker of gap junctions in NRK cells (16) (Fig. 3D). Taken together, the observed colocalization of Cx43 with TNTs, the voltage sensitivity of the conductance, and the reduced number of electrically coupled cells in the presence of MFA suggest that gap-junction proteins play a central role in the TNT-dependent electrical coupling of NRK cells.

TNT-Dependent Electrical Coupling Occurs Between Cells with Functional Gap Junctions. To address if TNT-dependent electrical coupling is a general characteristic of animal cells, we first investigated HEK293 cells. HEK293 cells form TNTs mainly by dislodgement (82%, $n = 13$ of 17 formation events) and to a minor extent by filopodial interplay (18%). TNT-connected HEK293 cell pairs were electrically coupled as indicated by DiBAC$_4$(3) fluorescence (Fig. 4 A and C) and Cx43 immunostaining was evident on only one end of a TNT connection (Fig. S3A, Top). Consistent with the latter observation, the TNT between HEK293 cells appeared to be continuous with the membrane of only one of the two cells (Fig. S3A, Middle) ($n = 50$). In primary human umbilical vein endothelial cells (HUVECs), TNT-dependent electrical coupling was also observed (Fig. 4 A and C) and Cx43 immunostaining was evident at only one end of the TNT connection (Fig. S3B, Top). As a positive control for the presence of functional gap junctions in both cell types, electrical coupling and dye transfer were recorded between abutting cells (Fig. S3 A and B, Bottom). In quail neuronal crest cells (NCCs) migrating from neural tube explants, identified by a specific marker HNK-1 (17) (Fig. S4A), TNTs formed via dislodgement ($n = 7$ of 7 formation events). Mechanical stimulation of TNT-connected cell pairs from these cultures revealed that only few of them were electrically coupled (Fig. 4 A and C). Similarly, a low percentage of electrically coupled cells was found for abutting NCC cell pairs (Fig. 4C). Immunofluorescence analysis showed that TNT-connected NCC cells were only in some cases positive for Cx43 (Fig. S4B, Top and Middle), whereas TNTs between NCC and non-NCC cells were always positive for Cx43 (Fig. S4B, Bottom). This finding suggests that only a subpopulation of NCC cells expresses gap junctions leading to electrical coupling.

The above results suggest that TNT-dependent electrical coupling is characteristic of cells that express both TNTs and functional gap junctions. To test this, we investigated a gap junction-deficient cell line, PC12 cells (18), which form TNTs by filopodial interplay (19). The absence of gap-junction communication between abutting cells was confirmed with both patch-clamp and Cascade Blue dye transfer experiments. For 23 pairs of TNT-connected PC12 cells, we observed no increase in DiBAC$_4$(3) fluorescence of the TNT-connected cell following mechanical stimulation (Fig. 4 A and C). In dual voltage-clamp recordings of TNT-connected PC12 cell pairs, we found no evidence of electrical coupling (Fig. 4B) ($n = 6$). These data support a model in which connexin channels are important mediators of TNT-dependent electrical coupling.

TNT-Transmitted Depolarization Signals Activate Low Voltage-Gated Ca²⁺ Channels in HEK293 Cells. To investigate whether the observed TNT-mediated electrical coupling could lead to measurable physiological changes, we simultaneously measured membrane potentials with DiBAC$_4$(3) and intracellular Ca^{2+} levels ($[Ca^{2+}]_i$) with the fluorescent calcium indicator X-rhod-1 in TNT-connected HEK293 cell pairs. Mechanical stimulation of one HEK293 cell always revealed a depolarization and an increase in $[Ca^{2+}]_i$ in the stimulated cell. However, calcium elevations were sometimes observed in cells which had no physical connection to the stimulated cell (Fig. S5, Upper). To eliminate these unspecific signals, we applied 100 µM suramin, a purinergic receptor blocker (20), which completely suppressed these calcium elevations (Fig. S5, Lower). In the presence of suramin, fast elevated calcium levels were observed in ~50% of TNT-connected HEK293 cells when the stimulated cell was depolarized (Fig. 5A, Top). In the remaining ~50% however, the TNT-connected cell did not show an increase in $[Ca^{2+}]_i$, even though the $[Ca^{2+}]_i$ was always strongly elevated in the stimulated cell (Fig. 5A, Middle). This finding, in conjunction with our finding that a 30 µm but not a 19 µm long TNT led to a change in $[Ca^{2+}]_i$ in the connected cell, excluded a length-limited diffusion of calcium from the stimulated cell via the TNT. Instead, we observed that the
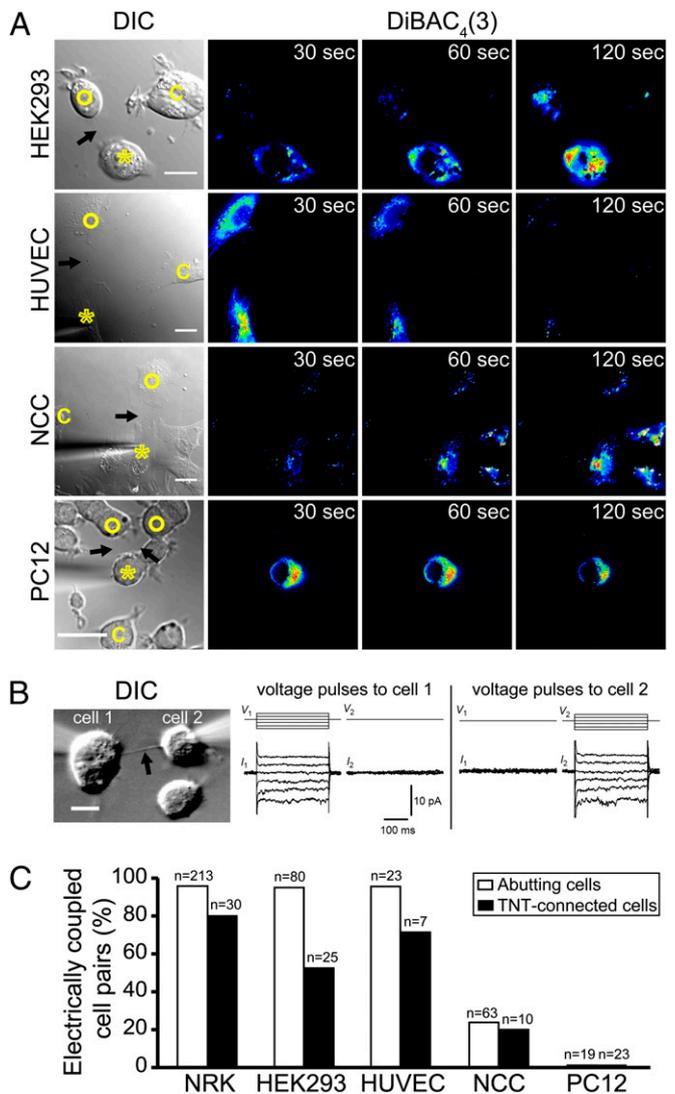
Fig. 4. TNT-dependent electrical coupling in different cell types. (A) TNT-connected cells are electrically coupled. The DIC images show the mechanically stimulated cells (asterisks), TNT-connected cells (open circles), TNTs (arrows), and control cells (c). The pseudocolored intensity images, generated by subtraction of the image before stimulation, depict increased fluorescence of DiBAC$_4$(3) of TNT-connected cell pairs at indicated times. (Scale bars, 20 µm.) (B) (Left) DIC image of TNT-connected PC12 cell pair during patch-clamp electrophysiological recording. (Scale bar, 10 µm.) (Center) With the TNT-connected PC12 cell pair in voltage-clamp (V_{hold} = 0 mV), a series of 300-ms voltage pulses (V_1) of −30 mV to +10 mV (in 10-mV increments; illustrated in upper traces) were applied to cell 1 while current responses were recorded from both cells (I_1 and I_2; lower traces). Depolarizing and hyperpolarizing voltage pulses applied to cell 1 result in outward and inward currents, respectively, in cell 1, and no change in current measured in cell 2. (Right) Same as in the Center, but voltage steps are applied to cell 2. No change in current was measured in cell 1. Traces are average of 10 repetitions. (C) Shown is the electrical coupling ratio of abutting and TNT-connected cell pairs of different cell types. After one cell was mechanically stimulated, the DiBAC$_4$(3) fluorescence of the abutting or TNT-connected cells was measured. The threshold applied to identify electrically coupled cells is described in Materials and Methods. n, number of cell pairs analyzed.

TNT-connected cells that displayed increased $[Ca^{2+}]_i$ also displayed an increase in their membrane potential that exceeded a ΔF_{max} of 0.2 during the first minute after stimulation (Fig. 5B, open black triangles).

The threshold-dependent correlation between the extent of depolarization and the increase in $[Ca^{2+}]_i$ suggested that voltage-gated Ca^{2+} channels were being activated. Because voltage-gated

CELL BIOLOGY

Ca^{2+} channels in HEK293 cells activate at a low voltage and, as such, have been compared with a T-type Ca^{2+} channel (21), we repeated the above experiments in the presence of 5 μM mibefradil, a selective blocker of low voltage-gated Ca^{2+} channels at this low concentration (22). Irrespective of the level of depolarization in the stimulated cell, no changes in $[Ca^{2+}]_i$ occurred in TNT-connected cells in the presence of mibefradil (Fig. 5A, Bottom, and B, red triangles). In contrast, NRK cells express an L-type Ca^{2+} channel that is activated at higher membrane potentials (23). When we repeated the above experiments with TNT-connected NRK cell pairs, we never observed changes in $[Ca^{2+}]_i$, as measured with X-rhod-1 (Fig. S6) ($n = 10$). This finding suggests that, under our stimulating conditions, TNT-mediated depolarizations can be large enough to activate low-threshold voltage-gated Ca^{2+} channels but are not sufficient to activate the higher threshold L-type Ca^{2+} channels in NRK cells.

Discussion

In this study we provide strong evidence that animal cells can be electrically coupled over long distances via TNTs and that gap junctions are needed for this communication (Fig. 5C). TNT-mediated electrical coupling was observed between all cell types that express Cx43, including NRK, HEK293, HUVEC, and NCC cells. We found no evidence for electrical coupling between TNT-connected PC12 cells, which do not express gap junctions. This result suggests that there are at least two different types of TNTs: those that interpose connexins and thus participate in electrical coupling, and those that lack connexins and do not display electrical coupling. Cx43 immunoreactivity was most frequently expressed at only one end of a TNT connecting two cells, implying a membrane border at that end of the TNT and a continuity of the TNT membrane with the other cell. The maximally observed conductance value was 1.3 nS for one TNT connection and, given a single channel conductance of 61 pS for Cx43 (24), this suggests that at least an equivalent of ~20 open channels were involved in the respective coupling. Thus, the TNT-dependent electrical coupling efficiency between cells is likely to be determined not only by the length and number of TNTs between cells but also by the number and open probability of the connexin channels present.

Our results suggest that ~80% of the TNTs between NRK cells mediate electrical coupling. We have demonstrated previously that ~50% of TNTs between NRK cells are involved in organelle transfer (5). This finding suggests that a number of TNTs are likely to be involved in both processes and raises the question as to the mechanism by which organelle transfer occurs between TNT-connected cells. Conceivable mechanisms might involve exo- and endocytotic events at the membrane interface, or a transient fusion of the TNT membrane with the target-cell membrane. Moreover, based on our data here, TNTs in PC12 cells are not permanently open at both ends, but instead form a membrane border (or interface) with one cell. This finding is seemingly in contrast with our previous finding that a few TNTs in PC12 cells showed opening at both ends evidenced by morphological evidence (3). These open-ended TNTs could reflect transient structures, which may facilitate short-lived organelle transfer as documented by long observation periods (3, 19). However, capturing these transient events by long-lasting electrical measurements may be difficult because of technical limitations. TNT-dependent transfer of organelle cargo between cells has been observed in a variety of different cell types (3, 5–7, 19), thus the mechanisms of transfer are of considerable interest for future studies.

Our result that TNT-mediated electrical coupling is of a magnitude sufficient to activate voltage-gated calcium channels in the recipient cell does not support a simple model of calcium diffusion (Fig. 5C). We observed that high $[Ca^{2+}]_i$ in the stimulated cells was not sufficient to evoke calcium signals in the TNT-connected cell if the transmitted depolarization was below a threshold value. However, two recent studies in dendritic and transfected HeLa cells found evidence for TNT-dependent intercellular calcium signaling via calcium diffusion through TNTs (25, 26). This finding suggests that different mechanisms of intercellular calcium signaling are likely to exist and may reflect the diversity of TNT structures and
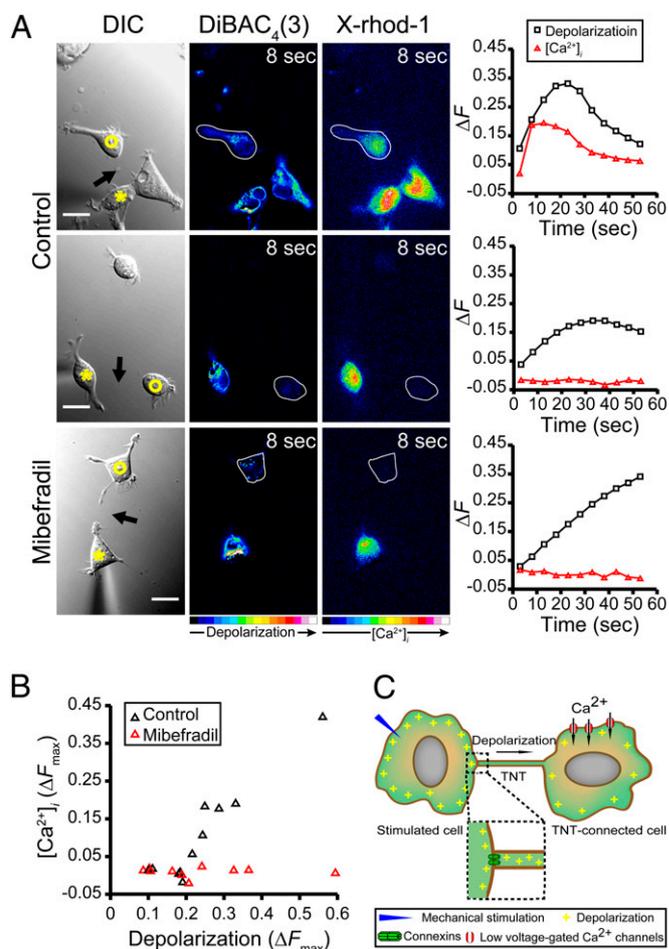
Fig. 5. TNT-mediated depolarization activates low voltage-gated Ca^{2+} channels in HEK293 cells. (A) The DIC images show the mechanically stimulated cells (asterisks), TNT-connected cells (open circles), and TNTs (arrows). The pseudocolored intensity images, generated by subtraction of the image before stimulation, depict the fluorescence changes of $DiBAC_4(3)$ (second column) and X-rhod-1 (third column) at indicated times after mechanical stimulation. The color bar indicates relative level of depolarization or $[Ca^{2+}]_i$ elevation. The corresponding fluorescence intensity changes (ΔF) of both $DiBAC_4(3)$ (black curves) and X-rhod-1 (red curves) of the TNT-connected cells were calculated (fourth column). The $[Ca^{2+}]_i$ of the TNT-connected cell is elevated along with the strong depolarization (Top), but not upon weak depolarization (Middle). No increase in $[Ca^{2+}]_i$ of TNT-connected cells displaying strong depolarization was observed in the presence of 5 μM mibefradil (Bottom). (Scale bars, 20 μm.) (B) Relation between depolarization and $[Ca^{2+}]_i$ increase of TNT-connected HEK293 cells. Each datapoint corresponds to the maximum fluorescence increase (ΔF_{max}) of $DiBAC_4(3)$ and X-rhod-1 in TNT-connected cells within 1 min after stimulation with ($n = 10$) or without 5 μM mibefradil ($n = 11$). All measurements were carried out in the presence of 100 μM suramin. (C) Proposed model for the TNT-dependent electrical coupling and opening of low voltage-gated Ca^{2+} channels. When one cell of a TNT-connected pair is depolarized by mechanical stimulation, the depolarization signal spreads through TNTs to the connected cell via gap junctions. Above a threshold of depolarization in the TNT-connected cells, low voltage-gated Ca^{2+} channels open and result in transient calcium signals.

functions in specific cell types (6, 7). Furthermore, our findings here open up the possibility that TNTs participate in physiologically relevant cell functions. In particular, the collective behavior of solitary or loosely attached migratory cells that follow the same tracks during diverse developmental processes could benefit from a long-distance signaling network. Cell-to-cell contacts via long "thin filopidia" have been observed in vivo within a stream of migrating NCC (27) and migration of cells during sea urchin gastrulation (28). Our result that some NCC cells were indeed electrically

coupled via TNTs suggests that TNTs could play an important role in the coordination of NCC migration.

In addition to the activation of voltage-gated ion channels, TNT-mediated electrical coupling may affect other downstream pathways and processes in connected cells, including the modulation of activity of small-molecule transporters (2) and the activation of enzymes, such as protein kinase A (29), PI3 kinase (2), or voltage-sensitive phosphatase (30). F-actin-rich membrane extensions connecting opposing cells at wound sites have been observed (31), as well as the activation of PI3 kinase during wound healing (2) and a membrane depolarization at the leading edge of wounds (32). This finding may suggest that membrane extensions/TNT-like structures propagate depolarization signals over long distances to synchronize the observed F-actin remodeling by activation of downstream signaling cascades during healing. Thus, our study provides evidence that the transfer of electrical signals via TNTs and the subsequent activation of physiologically relevant biophysical signals may provide a unique mechanism for long-distance cellular signaling.

Materials and Methods

Membrane Potential and $[Ca^{2+}]_i$ Imaging. For single membrane-potential measurements, cells were preloaded with 2 μM of DiBAC$_4$(3) (Sigma-Aldrich) at 37 °C for 45 min. Time-lapse fluorescence images were acquired before and after mechanical stimulation with excitation at 488 nm. For simultaneous measurement of $[Ca^{2+}]_i$ and membrane potential, cells were loaded with 0.3 μM X-rhod-1 AM (Molecular Probes) for 30 min, then with 2 μM DiBAC$_4$(3) at 37 °C for 30 min. Fluorescence images (excitation at 560/488 nm respectively) were obtained under the same conditions as single membrane-potential measurements, except that 100 μM suramin (Sigma-Aldrich) was present.

Electrophysiological Measurements. For patch-clamp recording, cell medium was replaced with (in mM): 145 NaCl, 10 glucose, 2.5 KCl, 2.5 CaCl$_2$, 1 MgCl$_2$, 5 Hepes (pH 7.4). Recording pipettes (5–7 MΩ) were filled with (in mM): 125 CsCl, 8 NaCl, 1 CaCl$_2$, 5 EGTA, 15 TEA-Cl, 4 MgATP, 10 Hepes (pH = 7.3). Dual whole-cell recordings were performed with an EPC9-dual patch-clamp amplifier controlled by PatchMaster software (HEKA Elektronik GmbH) as described previously (14).

More details of the methods can be found in SI Materials and Methods.

1. Levin M, Thorlin T, Robinson KR, Nogi T, Mercola M (2002) Asymmetries in H+/K+-ATPase and cell membrane potentials comprise a very early step in left-right patterning. *Cell* 111:77–89.
2. Levin M (2007) Large-scale biophysics: Ion flows and regeneration. *Trends Cell Biol* 17:261–270.
3. Rustom A, Saffrich R, Markovic I, Walther P, Gerdes HH (2004) Nanotubular highways for intercellular organelle transport. *Science* 303:1007–1010.
4. Onfelt B, Nedvetzki S, Yanagi K, Davis DM (2004) Cutting edge: Membrane nanotubes connect immune cells. *J Immunol* 173:1511–1513.
5. Gurke S, et al. (2008) Tunneling nanotube (TNT)-like structures facilitate a constitutive, actomyosin-dependent exchange of endocytic organelles between normal rat kidney cells. *Exp Cell Res* 314:3669–3683.
6. Gerdes HH, Carvalho RN (2008) Intercellular transfer mediated by tunneling nanotubes. *Curr Opin Cell Biol* 20:470–475.
7. Davis DM, Sowinski S (2008) Membrane nanotubes: Dynamic long-distance connections between animal cells. *Nat Rev Mol Cell Biol* 9:431–436.
8. Sowinski S, et al. (2008) Membrane nanotubes physically connect T cells over long distances presenting a novel route for HIV-1 transmission. *Nat Cell Biol* 10:211–219.
9. Eugenin EA, Gaskill PJ, Berman JW (2009) Tunneling nanotubes (TNT) are induced by HIV-infection of macrophages: A potential mechanism for intercellular HIV trafficking. *Cell Immunol* 254:142–148.
10. Gousset K, et al. (2009) Prions hijack tunnelling nanotubes for intercellular spread. *Nat Cell Biol* 11:328–336.
11. Chauveau A, Aucher A, Eissmann P, Vivier E, Davis DM (2010) Membrane nanotubes facilitate long-distance interactions between natural killer cells and target cells. *Proc Natl Acad Sci USA* 107:5545–5550.
12. Chinnery HR, Pearlman E, McMenamin PG (2008) Cutting edge: Membrane nanotubes in vivo: A feature of MHC class II+ cells in the mouse cornea. *J Immunol* 180:5779–5783.
13. Tokarz M, et al. (2005) Single-file electrophoretic transport and counting of individual DNA molecules in surfactant nanotubes. *Proc Natl Acad Sci USA* 102:9127–9132.
14. Veruki ML, Hartveit E (2002) AII (Rod) amacrine cells form a network of electrically coupled interneurons in the mammalian retina. *Neuron* 33:935–946.
15. González D, Gómez-Hernández JM, Barrio LC (2007) Molecular basis of voltage dependence of connexin channels: an integrative appraisal. *Prog Biophys Mol Biol* 94:66–106.
16. Harks EG, et al. (2001) Fenamates: A novel class of reversible gap junction blockers. *J Pharmacol Exp Ther* 298:1033–1041.
17. Tucker GC, Aoyama H, Lipinski M, Tursz T, Thiery JP (1984) Identical reactivity of monoclonal antibodies HNK-1 and NC-1: Conservation in vertebrates on cells derived from the neural primordium and on some leukocytes. *Cell Differ* 14:223–230.
18. van der Heyden MA, et al. (1998) Identification of connexin43 as a functional target for Wnt signalling. *J Cell Sci* 111:1741–1749.
19. Bukoreshtliev NV, et al. (2009) Selective block of tunneling nanotube (TNT) formation inhibits intercellular organelle transfer between PC12 cells. *FEBS Lett* 583:1481–1488.
20. Fischer W, Franke H, Gröger-Arndt H, Illes P (2005) Evidence for the existence of P2Y1,2,4 receptor subtypes in HEK-293 cells: reactivation of P2Y1 receptors after repetitive agonist application. *Naunyn Schmiedebergs Arch Pharmacol* 371:466–472.
21. Berjukow S, et al. (1996) Endogenous calcium channels in human embryonic kidney (HEK293) cells. *Br J Pharmacol* 118:748–754.
22. Martin RL, Lee JH, Cribbs LL, Perez-Reyes E, Hanck DA (2000) Mibefradil block of cloned T-type calcium channels. *J Pharmacol Exp Ther* 295:302–308.
23. de Roos AD, Willems PH, Peters PH, van Zoelen EJ, Theuvenet AP (1997) Synchronized calcium spiking resulting from spontaneous calcium action potentials in monolayers of NRK fibroblasts. *Cell Calcium* 22:195–207.
24. Valiunas V, Bukauskas FF, Weingart R (1997) Conductances and selective permeability of connexin43 gap junction channels examined in neonatal rat heart cells. *Circ Res* 80:708–719.
25. Watkins SC, Salter RD (2005) Functional connectivity between immune cells mediated by tunneling nanotubules. *Immunity* 23:309–318.
26. Hase K, et al. (2009) M-Sec promotes membrane nanotube formation by interacting with Ral and the exocyst complex. *Nat Cell Biol* 11:1427–1432.
27. Teddy JM, Kulesa PM (2004) In vivo evidence for short- and long-range cell communication in cranial neural crest cells. *Development* 131:6141–6151.
28. Miller J, Fraser SE, McClay D (1995) Dynamics of thin filopodia during sea urchin gastrulation. *Development* 121:2501–2511.
29. Zhang C, et al. (2004) Calcium- and dynamin-independent endocytosis in dorsal root ganglion neurons. *Neuron* 42:225–236.
30. Murata Y, Iwasaki H, Sasaki M, Inaba K, Okamura Y (2005) Phosphoinositide phosphatase activity coupled to an intrinsic voltage sensor. *Nature* 435:1239–1243.
31. Wood W, et al. (2002) Wound healing recapitulates morphogenesis in *Drosophila* embryos. *Nat Cell Biol* 4:907–912.
32. Chifflet S, Hernández JA, Grasso S (2005) A possible role for membrane depolarization in epithelial wound healing. *Am J Physiol Cell Physiol* 288:C1420–C1430.

CELL BIOLOGY